$CsPbBr_3$ Perovskite Nanocrystal Grown on MXene Nanosheets for Enhanced Photoelectric Detection and Photocatalytic CO_2 Reduction

Aizhao Pan,[,†] Xiaoqin Ma,[†] Shengying Huang,[†] Youshen Wu,[†] Mengjun Jia,[†] Peihua Wangyang,[‡] Ya Liu,[$] Yeming Shi,[‡] Ling He,[*,†] and Yi Liu[*,#]*

† Department of Chemistry, School of Science, Xi'an Jiaotong University, Xianning West Road, 28, Xi'an, 710049, China.

‡ College of Optoelectronic Technology, Chengdu University of Information Technology, Chengdu, 610225, China

$ International Research Center for Renewable Energy, State Key Laboratory of Multiphase Flow in Power Engineering, Xi'an Jiaotong University, Shaanxi 710049, China

The Molecular Foundry, Lawrence Berkeley National Laboratory, Berkeley, California 94720, United States.

Corresponding Author

*Email: panaizhao2017032@xjtu.edu.cn, yliu@lbl.gov.

ABSTRACT: All-inorganic $CsPbX_3$ (X = Cl, Br or I) perovskite nanocrystals have attracted extensive interest recently due to their exceptional optoelectronic properties. In an effort to improve the charge separation and transfer following efficient exciton generation in such nanocrystals, novel functional nanocomposites were synthesized by the *in-situ* growth of $CsPbBr_3$ perovskite nanocrystals on two-dimensional MXene nanosheets. Efficient excited state charge transfer occurs between $CsPbBr_3$ NCs and MXene nanosheets, as indicated by significant photoluminescence (PL) quenching and much shorter PL decay lifetimes compared with pure $CsPbBr_3$ NCs. The as-obtained $CsPbBr_3$/MXene nanocomposites demonstrated increased photocurrent generation in response to visible light and X-ray illumination, attesting to the potential application of these heterostructure nanocomposites for photoelectric detection. The efficient charge transfer also renders the $CsPbBr_3$/MXene nanocomposite an active photocatalyst for the reduction of CO_2 to CO and CH_4. This work provides a guide for exploration of perovskite materials in next-generation optoelectronics, such as photoelectric detectors or photocatalyst.

~~TOC GRAPHICS~~ Table of Contents image

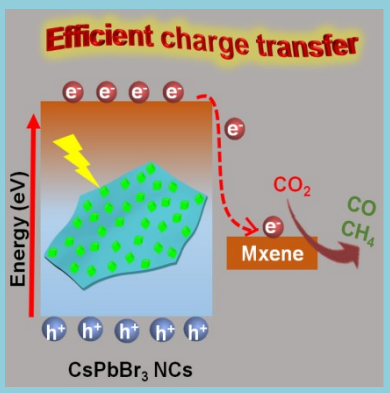

KEYWORDS: $CsPbBr_3$ perovskite nanocrystals, fluorescence quenching, MXene nanosheets, photoinduced charge transfer, photoresponses

All-inorganic cesium lead halide ($CsPbX_3$, X = Cl, Br, I) perovskite nanocrystals (NCs) have received enormous attention recently because of their unique optoelectronic properties, such as high photoluminescence efficiencies (>90%), a wide range of colors, narrow emission bands, and highly tunable bandgaps.[1-5] These remarkable features make $CsPbX_3$ perovskite NCs excellent material candidates for next-generation optoelectronic applications such as light-emitting diodes (LEDs), anti-counterfeit inks, and lasers.[6-10] Recent efforts have further demonstrated that $CsPbX_3$ perovskite NCs are promising materials for photodetectors due to their high atomic number and high μτ product (where μ and τ are the carrier mobility and carrier lifetime, respectively).[8, 9, 11-16]

Low-dimensional materials (e.g., phosphorene, molybdenum disulfide, graphene, and MXenes), on the other hand, represent another frontier research thrust in optoelectronics on account of their layer-dependent electronic structures.[17-21] Heterostructures integrating low-dimensional

materials with perovskite NCs can lead to enhanced optoelectronic properties, as having been demonstrated in nanocomposites based on $CsPbBr_3$ NCs and black phosphorus, reduced graphene oxide (RGO) or NH_x-rich porous g-C_3N_4 nanosheets,[12, 21-23] where fast separation and transfer of photo-generated electrons occurs to result in enhanced photoresponse for photodetectors and photocatalytic CO_2 reduction.[21-24]

More recently, a unique family of two-dimensional layered $Ti_3C_2T_x$ (where T_x represents surface terminations such as fluorine, oxygen, and hydroxyl groups) MXene materials has drawn great attention because of their excellent metallic conductivity, high volumetric capacitance (900 F cm^{-3}), flexible interlayered regulation, and hydrophilic surfaces.[19, 25-27] Such properties have allowed these materials to be used in a wide range of applications, including energy electrodes, energy storage, catalysts, gas separation, and cell imaging.[19, 25, 26, 28-30] It has been incorporated in various heterostructures, such as MoS_2/MXene,[20] Bi_2WO_6/MXene,[31] black phosphorus quantum dots/MXene,[27] and MXene-rHGO_3 nanocomposites[32], though its coordinated use for perovskite NC-based heterostructures has remained unexplored.

Herein, we demonstrate a facile strategy for constructing $CsPbBr_3$/MXene nanocomposites by growing $CsPbBr_3$ NCs onto MXene nanosheets, yielding uniform dispersion of $CsPbBr_3$ NCs and tunable PL. The charge transfer properties of the nanocomposites with various ratio of $CsPbBr_3$ NCs and MXene nanosheets were studied using time-resolved photoluminescence

(TRPL) spectroscopy and decay lifetime measurements. The resulting $CsPbBr_3$/MXene nanocomposites have demonstrated enhanced performance in photodetection of visible light and X-ray illumination, and photocatalytic reduction of CO_2.

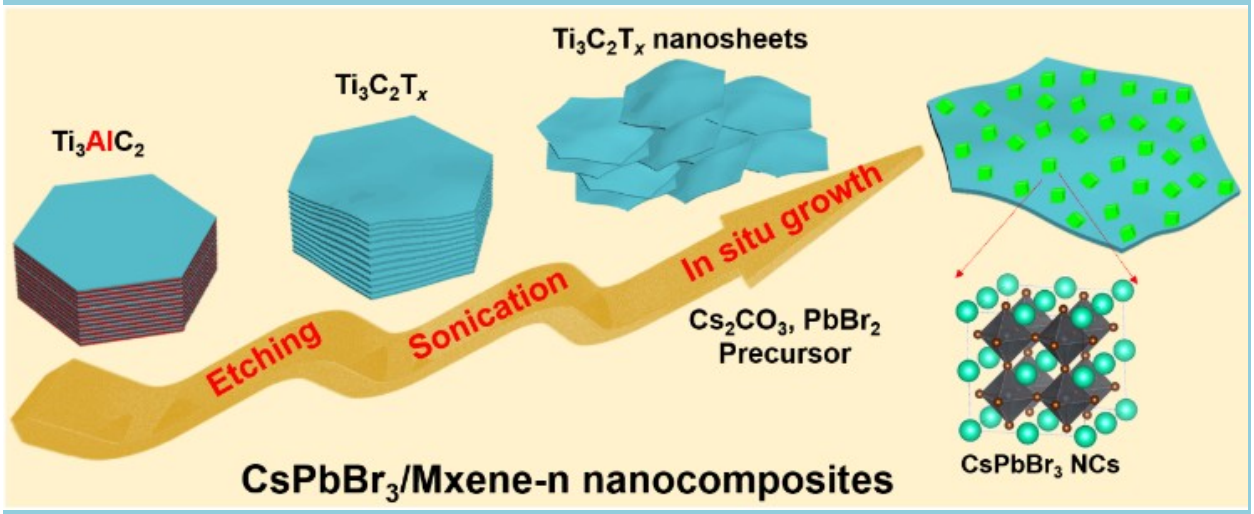

Scheme 1. Schematic illustration of the *in-situ* growth process of $CsPbBr_3$ perovskite NCs on exfoliated MXene nanosheets.

The overall synthetic method used to obtain $CsPbBr_3$/MXene nanocomposites is presented in **Scheme 1**, which involves three separate processes: etching to obtain multilayered $Ti_3C_2T_x$, sonication to exfoliate and obtain monolayer $Ti_3C_2T_x$ (MXene) nanosheets, and the *in situ* growth of $CsPbBr_3$ nanocrystals on MXene nanosheets. Briefly, monolayer MXene nanosheets were synthesized following a reported procedure via a facile two-step approach (see Supporting Information). The multilayered $Ti_3C_2T_x$ of dark black powder was firstly synthesized by the selective etching of Al atoms from Ti_3AlC_2 powder using an HCl-HF solution, which was subsequently delaminated into monolayered nanosheets (MXene) via probe-sonication

(Scheme 1).[19, 25] Gradient centrifugation was used to collect MXene monolayered flakes by removing the multilayered $Ti_3C_2T_x$ which settled to the bottom. To ensure sure no water remained in MXene nanosheets which could potentially degrade $CsPbBr_3$ NCs, the MXene nanosheets were washed and purified by dispersing and centrifuging them with DMF and toluene alternately three times before being dried in a vacuum oven for 24 h.

$CsPbBr_3$/MXene nanocomposites were fabricated by growing $CsPbBr_3$ nanocrystals on MXene nanosheets at a certain molar ratio using a modified *in situ* growth protocol.[12] It is hypothesized that the preferential surface terminations such as fluorine, oxygen, and hydroxyl groups on the MXene are inclined to interact with OA/OLA, by forming kinetically favorable nucleation points for capturing $PbBr_2$ precursors. The expected nanocrystals will grow at the nucleation sites with the cesium precursor injected and free $PbBr_2$ diffused. In a typical procedure, $PbBr_2$ (69 mg), oleic acid (OA, 0.30 mL), and oleylamine (OLA, 0.30 mL) were pre-dissolved in ODE (5 mL) at 150 ºC. The MXene nanosheet (10, 20, 30 or 50 mg) suspensions in DMF (1 mL) were then injected into the above ODE solution under an N_2 atmosphere, followed by the addition of cesium oleate (0.4 mL, 0.125 M in ODE) under vigorous stirring. The reaction was quenched after 10 seconds, and then subjected to three to five cycles of centrifugation/re-dispersion in hexanes. The non-bound NCs in the system were easily purified and removed by centrifugation, while the NCs adhered to the MXene nanosheets were isolated as precipitates from the reaction mixture and dried in vacuum

overnight before use.[22] The resulting composites were named as $CsPbBr_3$/MXene-n (n = 10, 20, 30, 50), with n corresponding to the different amount of MXene used for the synthesis, respectively.

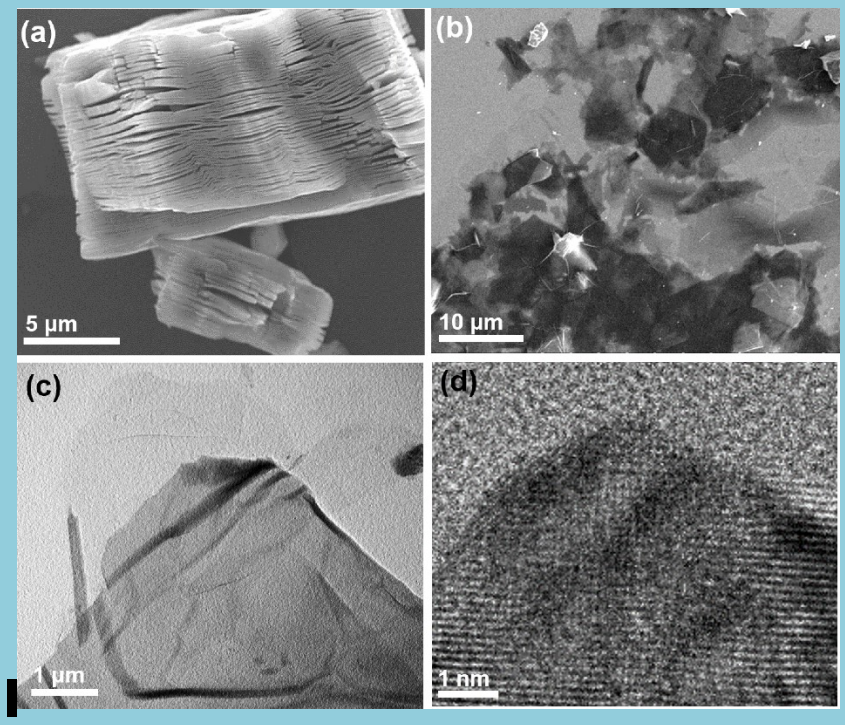

Figure 1. Scanning electron microscopy (SEM) images of multilayered $Ti_3C_2T_x$ (a) and mono-layered $Ti_3C_2T_x$ (MXene) nanosheets (b). (c) High-magnification transmission electron microscopy (TEM) image of mono-layered $Ti_3C_2T_x$ nanosheets. (d) High-resolution (HR) TEM image of mono-layered $Ti_3C_2T_x$ nanosheets.

The morphologies of the as-prepared multilayered $Ti_3C_2T_x$ and mono-layered $Ti_3C_2T_x$ (MXene) nanosheets were analyzed by scanning electron microscopy (SEM) and transmission electron microscopy (TEM). Figure 1a showed the SEM image of a fanned-out multilayered $Ti_3C_2T_x$ after the selective etching of Al atoms from Ti_3AlC_2, which was further confirmed in

Figure S1. The energy-dispersive spectroscopy (EDS) mapping images of oxygen (O), titanium (Ti), and fluorine (F) of the multilayered $Ti_3C_2T_x$ samples showed no signals from aluminum (Al), implying successful etching (Figure S2).[19] The SEM images of the exfoliated MXene nanosheets revealed electron-transparent foils with thin, smooth surfaces and diameters ranging from 100 nanometers to several micrometers (Figure 1b). MXene nanosheets were also confirmed to be thin and electron transparent by TEM, with a thickness similar to graphene, and local regions tended to fold due to their high flexibility and elasticity (Figure 1c). Figure 1d showed a high-resolution TEM image of MXene nanosheets, which further confirmed their graphene-like morphology and structures, consistent with the literature. [18, 19]

Figure 2a shows a low-magnification TEM image of the $CsPbBr_3$/MXene-20 nanocomposites. Many cubic $CsPbBr_3$ NCs were visibly dispersed on the surface of MXene nanosheets without apparent agglomeration. The NCs retained their regular cubic shapes, with an average size about 25 nm as determined from the size distribution statistics of the TEM images (Figure 2a and S3). The surface NCs were comparatively larger than unbound solution grown NCs, but similar to NCs (20-30 nm) grown on RGO surfaces that were previously reported, possibly due to Ostwald ripening.[12] Moreover, when the concentrations of $PbBr_2$ and cesium oleate precursors were kept constant while the MXene content was varied, the composition of the resulting $CsPbBr_3$/MXene-n nanocomposites changed accordingly (see Supporting Information). TEM images of these nanocomposites showed increasing NC

amounts on the MXene nanosheets as the MXene content decreased (Figure S4).

High-magnification TEM images of the as-obtained $CsPbBr_3$/MXene-20 nanocomposites in Figure 2b further confirmed the distributed presence of cubic shaped NCs on nanosheets. Additionally, the HR-TEM image in Figure 2c displayed a typical crystal lattice of $CsPbBr_3$ NCs, with a *d*-spacing of about 0.58 nm. This corresponds well to the (110) planes of $CsPbBr_3$ crystals, confirming the high crystallinity of the as-grown $CsPbBr_3$ NC.[1, 4] Furthermore, the TEM-EDX elemental mapping images indicated the distribution of Ti, Pb, Br, and Cs (Figure 2d-h), further confirming the growth of $CsPbBr_3$ NCs on the thin MXene nanosheets. The formation of the $CsPbBr_3$/MXene-20 nanocomposite and distribution of $CsPbBr_3$ NCs on the MXene nanosheets also corroborated with the SEM-EDX elemental mapping (Figure S5).

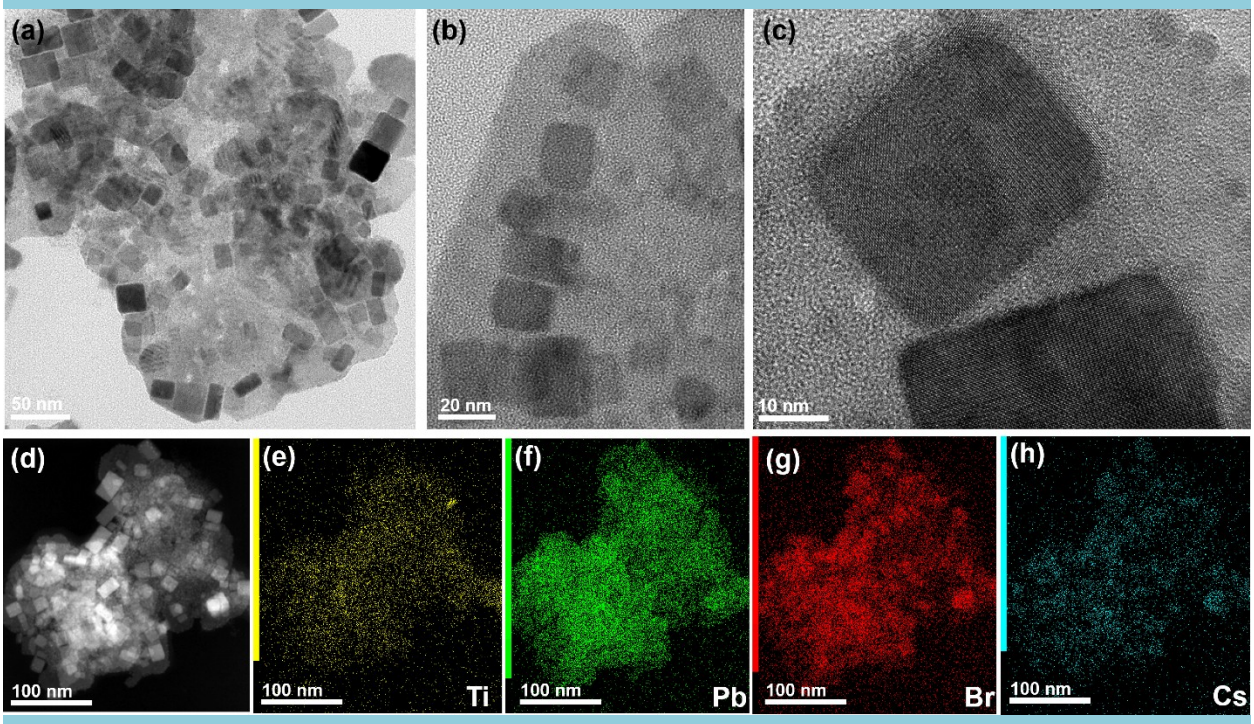

Figure 2. TEM (a), high-magnification TEM (b), and high-resolution TEM (c) images of the $CsPbBr_3$/MXene-20 nanocomposite. STEM image (d) along with the TEM energy-dispersive X-ray (EDX) elemental mapping profiles (e-h) of Ti, Pb, Br, and Cs of selected areas of the $CsPbBr_3$/MXene-20 nanocomposite.

The crystal structures of the $CsPbBr_3$/MXene-20 nanocomposite and MXene were determined by powder X-ray diffraction (PXRD) in Figure 3a. Compared with the diffraction peaks of MXene nanosheets (red line), the $CsPbBr_3$/MXene-20 nanocomposite showed both primary MXene diffraction peaks and additional new peaks, such as these major ones appeared at 21.5° and 30.5° which corresponded to the orthorhombic phase of $CsPbBr_3$ NCs.[1] Furthermore, X-ray photoelectron spectroscopy (XPS) spectra (Figures 3b and S6) were used to characterize the elemental composition of the $CsPbBr_3$/MXene-20 nanocomposite and compared against the MXene nanosheet spectrum. For MXene-only samples, peaks corresponding to F*1s*, O*1s*, C*1s*, and Ti*2p* were observed, which were expected for MXene nanosheets (Ti_3C_2) terminated with O, OH, and/or F groups.[19] In the $CsPbBr_3$/MXene-20 nanocomposite, additional peaks corresponding to Cs*3d*, Pb*4f*, and Br*3d* binding energies were detected, consistent with the presence of $CsPbBr_3$ NCs in the nanocomposites.[10] Raman spectra (λ = 633 nm) demonstrated obvious peaks shift of the Raman modes of MXene in the case of the $CsPbBr_3$/MXene-20 nanocomposite, which further confirm the external molecular interactions between the terminal groups and the ligands-capped NCs.[22]

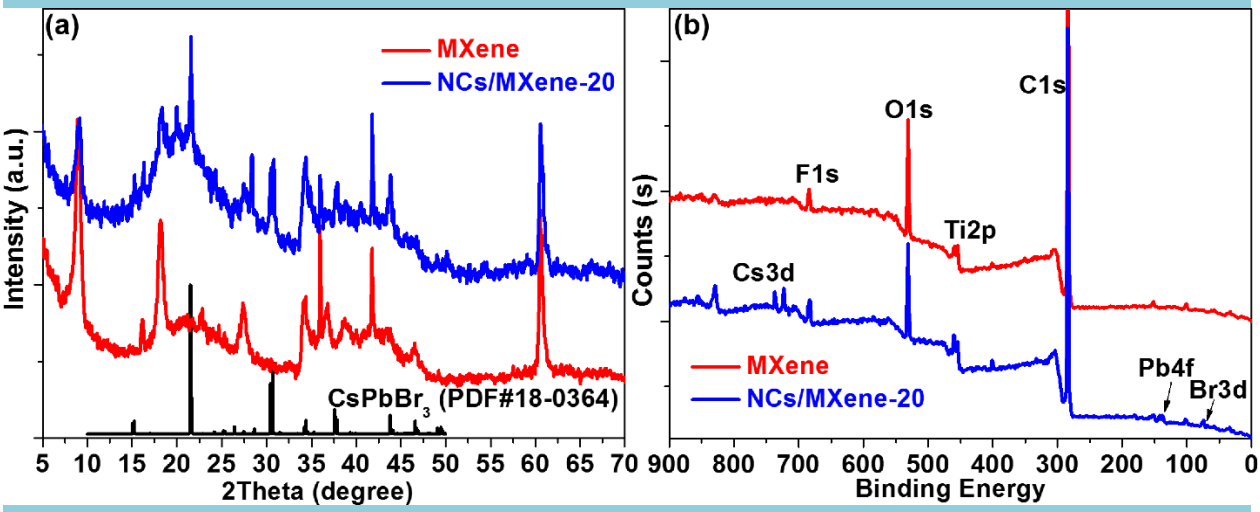

Figure 3. Powder X-ray diffraction (PXRD) patterns (a) and X-ray photoelectron spectroscopy (XPS) spectra (b) of mono-layered $Ti_3C_2T_x$ (MXene) and $CsPbBr_3$/MXene-20 nanocomposite.

The optical spectra of $CsPbBr_3$ NCs and $CsPbBr_3$/MXene-n nanocomposites with different MXene ratios were shown in Figure 4. A band edge at 500 nm was clearly observed in the absorption spectra of all the $CsPbBr_3$/MXene-n nanocomposites with different MXene compositions, which was nearly identical to that of free $CsPbBr_3$ NCs in Figure 4a, suggesting that the sizes of NCs ~~are~~were similar. Upon successively increasing the amount of MXene from 0 mg to 50 mg, the absorption spectra of the $CsPbBr_3$/MXene-n nanocomposites retained their native $CsPbBr_3$ NCs behavior. Figure 4b shows the steady-state photoluminescence (PL) spectra of as-obtained $CsPbBr_3$/MXene-n nanocomposites with different MXene concentrations. For comparison, the PL spectrum of the free $CsPbBr_3$ NCs exhibited a strong emission peak at 522 nm, and the full width at half maximum (FWHM) was a relatively narrow 21 nm.[1] However, when 10 mg MXene was used, the

corresponding emission peak of the $CsPbBr_3$/MXene-10 nanocomposites was weakened and the photoluminescence quantum yield (PLQY) was decreased from 86% ~~of~~for the pure $CsPbBr_3$ NCs to 27% for the composite, implying an obvious photoluminescence quenching effect. In addition, no prominent photoluminescence peaks appeared, nor were any changes observed in the $CsPbBr_3$ NCs/MXene nanocomposites, by referring to the energy transfer process, which clearly rules out the energy transfer induced quenching mechanism. [22] Thus, t~~T~~his quenching phenomenon was attributed to the transfer of photo-generated carriers between $CsPbBr_3$ NCs and MXene.[12, 21, 24] $CsPbBr_3$/MXene-10 exhibited an obvious blue shift from 522 nm to 515 nm (Figure 4c) compared to the free NCs, possibly attributed to the Burstein-Moss effect.[33, 34] As the MXene content increased successively, PL intensity decreased monotonically (the corresponding PLQYs decreased to 11% ~~of~~for $CsPbBr_3$/MXene-20 and less than 5% ~~of~~for $CsPbBr_3$/MXene-30/50), accompanied by consistent PL blue shift. Specifically, the emission peak of $CsPbBr_3$/MXene-50 shifted from 522 nm to 496 nm, similar to that reported for NCs on GO,[21] while the maximum photoluminescence quenching efficiency exceeds more than 90%.

The photoluminescence quenching and blue shift indicate intimate integration and interaction between the $CsPbBr_3$ NCs and MXene nanosheets. Time-resolved photoluminescence (TRPL, Figure 4d) measurements were further carried out to study the quenching effect between $CsPbBr_3$ NCs and MXene nanosheets. The decay traces were fitted using a two-~~-~~exponential

decay model [12] and the parameters ~~are~~were listed in Table S1. Compared against the PL lifetime (τ_{ave}) of the free $CsPbBr_3$ NCs at 18.8 ns, the PL lifetime decreased to 4.1 ns, 1.7 ns, 0.27 and 0.21 ns for $CsPbBr_3$/MXene-10, $CsPbBr_3$/MXene-20, $CsPbBr_3$/MXene-30 and $CsPbBr_3$/MXene-50, respectively. The shorter average PL lifetime of $CsPbBr_3$/MXene-n nanocomposites than the free $CsPbBr_3$ NCs suggested an efficient non-radiative pathway between MXene and $CsPbBr_3$ NCs, as was similarly observed in other NC–2D material composites,[12, 22, 24] which was ascribable to photo-induced electron transfer from $CsPbBr_3$ NCs to MXene. The relative energy level alignment between the $CsPbBr_3$ NCs and MXene nanosheets further supports an efficient charge transfer. As shown in Figure 5c, the conduction band offset (1.~~0~~5 eV) between the two components can effectively drive the separation of the photo-generated excitons in $CsPbBr_3$ NCs and transfer the electrons to MXene nanosheets.[35-38]

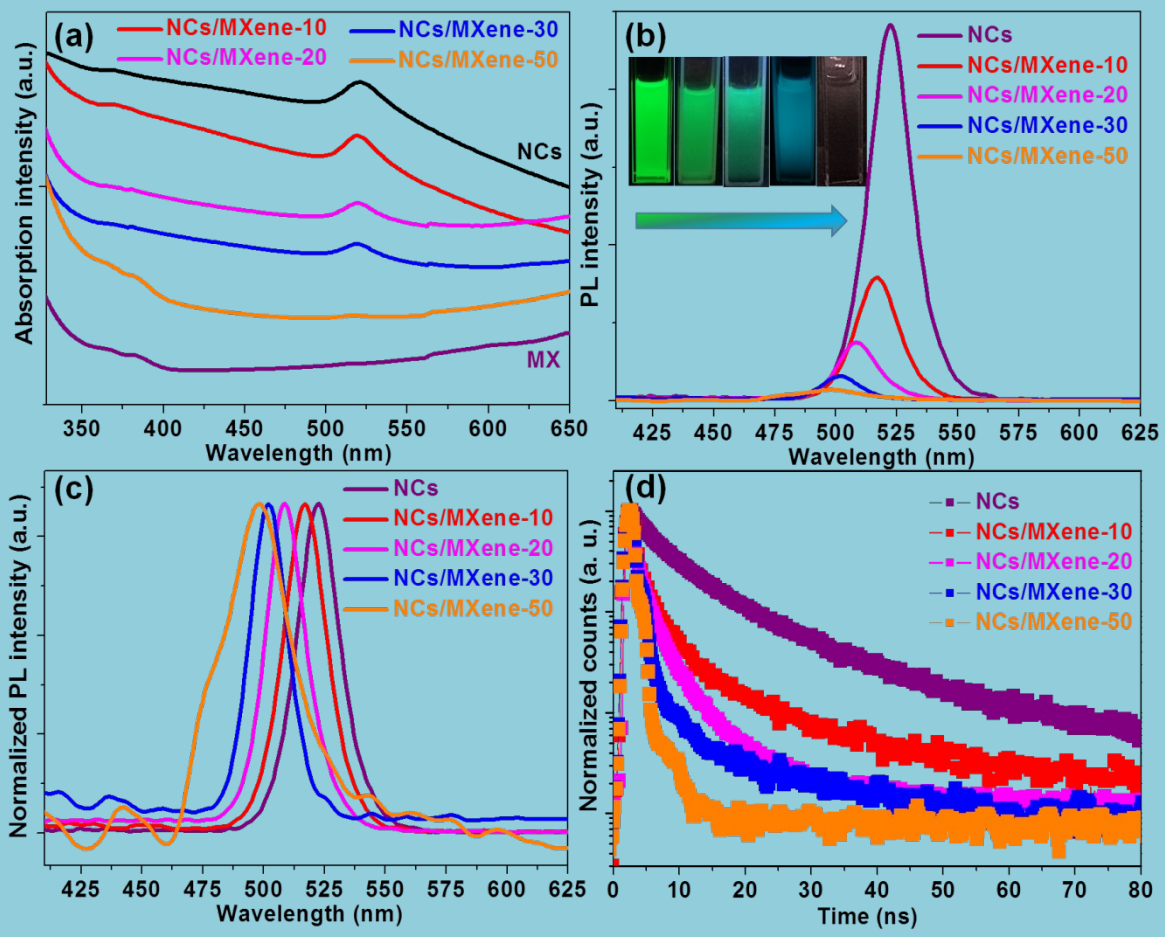

Figure 4. (a) Optical absorption spectra of MXene, $CsPbBr_3$ NCs and $CsPbBr_3$/MXene-n with different compositions. The photoluminescence spectra before (b) and after normalization (c) of $CsPbBr_3$ NCs and $CsPbBr_3$/MXene-n. Insets in (a) are images of the corresponding nanocomposites under 365 nm UV light. (d) PL decay of $CsPbBr_3$ NCs and $CsPbBr_3$/MXene-n.

Additionally, the photo-induced electron transfer from $CsPbBr_3$ NCs to MXene was further confirmed by photoconductivity measurements. Photoconduction devices were fabricated by depositing the nanocomposites onto interdigitated electrodes (Supporting Information, Figure ~~S7~~S8). The current-time (I-T) characteristics was subsequently evaluated under a white

light-emitting diode (WLED) or X-ray illumination.[12, 22] For comparison, the interdigitated electrodes were coated with MXene nanosheets and measured under white light illumination (Figure ~~S8~~S9). No measurable current changes were observed before and after illumination for the MXene-only devices, possibly due to low density of photo-generated carriers in MXene.[36] No working control devices based on $CsPbBr_3$ NCs were available as we were unable to obtain continuous films of $CsPbBr_3$ NCs.[12] In contrast, a significant photocurrent enhancement was observed in the device fabricated using $CsPbBr_3$/MXene-20 (Figure 5a) compared to the MXene-based device in which no photocurrent was detected under the same sweep voltage range. The $CsPbBr_3$/MXene-20 nanocomposite-based device exhibited sensitive rising and decaying times of 0.357 s and 0.361 s, respectively (Figure ~~S9~~S10), when light was turned on and off, which were shorter than that of NCs on RGO (0.417 s and 0.414 s) and free NCs (about 0.83 s).[12] Furthermore, this rapid response can be repeated for multiple cycles (Figure 5a). Similar photocurrent responses were observed when the same device was exposed to X-ray illumination (powder exposure-rate: 0.19 mGy/h) at zero bias (Figure 5b). Though further optimization is needed to improve the photocurrent generation, including the sensitivity, cycling lifetime, and stabilities [12, 22], the photo-induced current responses suggest effective carrier generation and transfer within the $CsPbBr_3$ NC/MXene-n nanocomposites under light or X-ray illumination.

The efficient charge-transfer in $CsPbBr_3$ NCs/MXene-20 nanocomposite under excitation prompted us to test its viability for photocatalytic CO_2 reduction. The proof-of-concept experiment was carried out in a sealed reaction vessel under simulated solar light illumination (300 W Xe lamp with a cut off filter >420 nm). Ethyl acetate was chosen as the solvent as CO_2 is highly soluble in ethyl acetate, and the $CsPbBr_3$ NCs remain stable in ethyl acetate due to its mild polarity.[21, 23] Only insignificant amount of CO was originated from photo-oxidation of ethyl acetate.[21, 23] After the solar irradiation, both CO and CH_4 were detected as the main conversion products (Figure 5d), with no H_2 and other products detected, indicating a highly selective reduction of CO_2 into CO and CH_4. The yields of the obtained CO and CH_4 increased linearly with time (Figure ~~S10~~S11). Particularly, $CsPbBr_3$ NCs/MXene-20 nanocomposites exhibited high CO and CH_4 formation rate of 26.32 and 7.25 $\mu mol \cdot g^{-1} \cdot h^{-1}$, respectively (Figure 5d), comparable or superior than that of free $CsPbBr_3$ NCs (<4.4 $\mu mol \cdot g^{-1} \cdot h^{-1}$) and some other newly developed $CsPbBr_3$ NCs-based heterostructure photocatalysts (Table S2).[21, 23, 39-42]

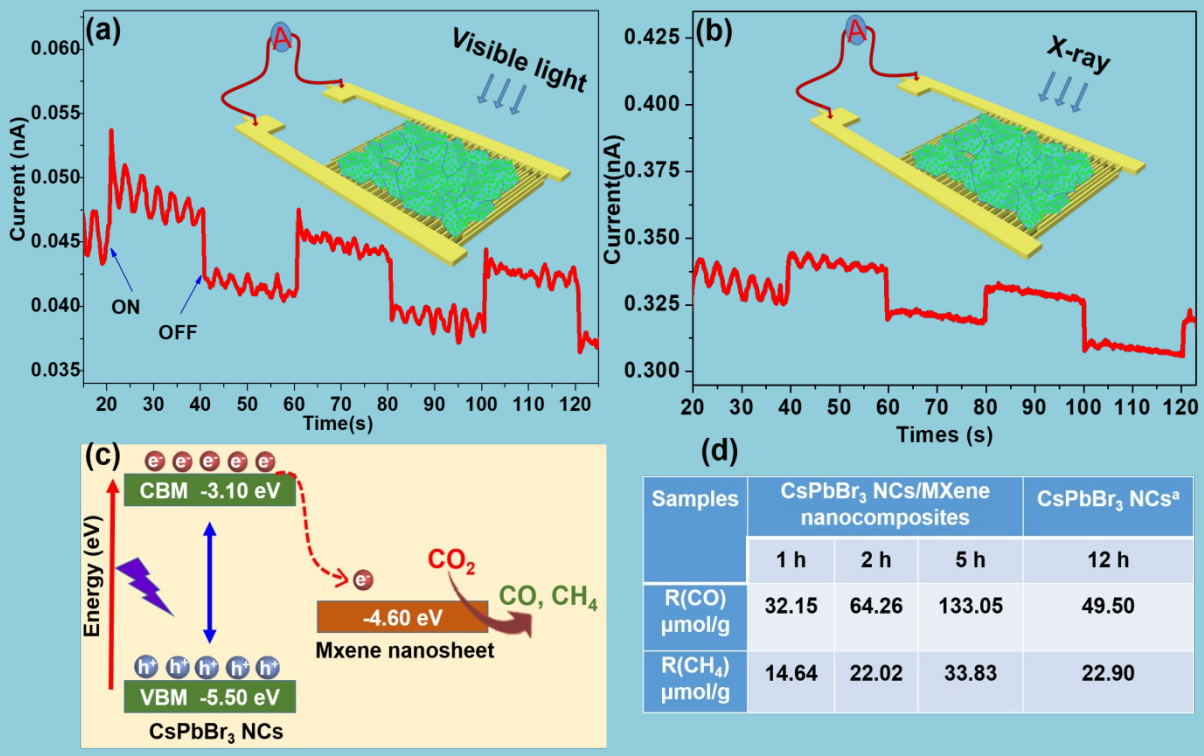

Samples	$CsPbBr_3$ NCs/MXene nanocomposites			$CsPbBr_3$ NCs[a]
	1 h	2 h	5 h	12 h
R(CO) μmol/g	32.15	64.26	133.05	49.50
$R(CH_4)$ μmol/g	14.64	22.02	33.83	22.90

Figure 5. Photocurrent response of devices based on $CsPbBr_3$ NCs/MXene-20 under white LED (a) and X-ray (b) illumination. Insets are the corresponding device schematics. (c) Schematic illustration of the relative energetic diagram of the $CsPbBr_3$ NCs/MXene-n heterostructures suitable for photocatalytic CO_2 reduction. (d) Summary of the products from photocatalytic CO_2 reduction under constant illumination of $CsPbBr_3$/MXene-20. [a] in (d) are data from previous references using $CsPbBr_3$ NCs as the photocatalyst.[21]

In conclusion, we have explored the synthesis of $CsPbBr_3$ NC/MXene-n nanocomposites by *in situ* growth of $CsPbBr_3$ NCs on the surface of monolayered MXene nanosheets. Efficient fluorescence quenching of the

$CsPbBr_3$ NCs, together with time-resolved photoluminescence lifetime and photoconductivity measurements, confirmed efficient charge transfer between MXene and $CsPbBr_3$ NCs. The $CsPbBr_3$/MXene nanocomposite-based devices displayed enhanced and sensitive photoresponse to visible light and X-ray illumination. In addition, the $CsPbBr_3$/MXene nanocomposites have shown high photocatalytic activity for selective reduction of CO_2 to CO and CH_4. The efficient charge-transfer in the $CsPbBr_3$/MXene nanocomposite and their application in photodetectors and photocatalytic applications lays the foundation for further research into high performance photocatalysts and sensors based on this class of novel heterostructured nanocomposites.

ASSOCIATED CONTENT

ACKNOWLEDGMENTS

This work was primarily supported by the National Natural Science Foundation of China (NSFC Grants 51802254, 51873173), the China Postdoctoral Science Foundation Funded Project (2017M623149, 2019T120902), the Fundamental Research Funds for the Central Universities (xjj2018053) and Shaanxi province Youth Foundation (2018JQ5011). Work at the Molecular Foundry was supported by the Office of Science, Office of Basic Energy Sciences, of the U.S. Department of Energy under Contract No. DE-AC02-05CH11231. The authors also wish to express their gratitude to the MOE Key Laboratory for Nonequilibrium Condensed Matter and Quantum Engineering of Xi'an Jiaotong University.

Supporting Information.

The Supporting Information is available free of charge on the ACS Publications website at XXX.

Synthetic details of $CsPbBr_3$ NCs, $Ti_3C_2T_x$ MXene nanosheets, $CsPbBr_3$/MXene-n nanocomposites; design of the photo-conductance devices; experimental of photocatalytic CO_2 reduction; TEM, HAADF-STEM/EDX mappings and XPS spectra of multilayered $Ti_3C_2T_x$ nanosheets and the $CsPbBr_3$/MXene-n nanocomposites. Time-dependent photoelectric current response and recovery time; Time courses of CO_2 reduction product CO and CH_4 evolution by $CsPbBr_3$ NCs/MXene nanocomposites (PDF)

AUTHOR INFORMATION

The manuscript was written through contributions of all authors. All authors have given approval to the final version of the manuscript.

Corresponding Author

*Email: panaizhao2017032@xjtu.edu.cn, yliu@lbl.gov, heling@mail.xjtu.edu.cn.

Notes

The authors declare no competing financial interest.

ACKNOWLEDGMENT

This work was primarily supported by the National Natural Science Foundation of China (NSFC Grants 51802254, 51873173), the China

~~Postdoctoral Science Foundation Funded Project (2017M623149, 2019T120902), the Fundamental Research Funds for the Central Universities (xjj2018053) and Shaanxi province Youth Foundation (2018JQ5011). Work at the Molecular Foundry was supported by the Office of Science, Office of Basic Energy Sciences, of the U.S. Department of Energy under Contract No. DE-AC02-05CH11231. The authors also wish to express their gratitude to the MOE Key Laboratory for Nonequilibrium Condensed Matter and Quantum Engineering of Xi'an Jiaotong University.~~

REFERENCES

(1) Protesescu, L.; Yakunin, S.; Bodnarchuk, M. I.; Krieg, F.; Caputo, R.; Hendon, C. H.; Yang, R. X.; Walsh, A.; Kovalenko, M. V. Nanocrystals of Cesium Lead Halide Perovskites ($CsPbX_3$, X = Cl, Br, and I): Novel Optoelectronic Materials Showing Bright Emission with Wide Color Gamut. *Nano Lett.* **2015**, *15*, 3692-3696.

(2) Yakunin, S.; Protesescu, L.; Krieg, F.; Bodnarchuk, M. I.; Nedelcu, G.; Humer, M.; De Luca, G.; Fiebig, M.; Heiss, W.; V. Kovalenko, M. Low-threshold Amplified Spontaneous Emission and Lasing from Colloidal Nanocrystals of Caesium Lead Halide Perovskites. *Nat. Commun.* **2015**, *6,* 8056-8063.

(3) Akkerman, Q. A.; D'Innocenzo, V.; Accornero, S.; Scarpellini, A.; Petrozza, A.; Prato, M.; Manna, L. Tuning the Optical Properties of Cesium Lead Halide Perovskite Nanocrystals by Anion Exchange Reactions. *J. Am. Chem. Soc.* **2015**, *137*, 10276-10281.

(4) Swarnkar, A.; Chulliyil, R.; Ravi, V. K.; Irfanullah, M.; Chowdhury, A.; Nag, A. Colloidal $CsPbBr_3$ Perovskite Nanocrystals: Luminescence beyond Traditional Quantum Dots. *Angew. Chem. Int. Edit.* **2015**, *54*, 15424-15428.

(5) Yang, D.; Cao, M. H.; Zhong, Q. X.; Li, P. L.; Zhang, X. H.; Zhang, Q. All-inorganic Cesium Lead Halide Perovskite Nanocrystals: Synthesis, Surface

Engineering and Applications. *J. Mater. Chem. C* **2019**, *7*, 757-789.
(6) Song, J. Z.; Li, J. H.; Li, X. M.; Xu, L. M.; Dong, Y. H.; Zeng, H. B. Quantum Dot Light-Emitting Diodes Based on Inorganic Perovskite Cesium Lead Halides ($CsPbX_3$). *Adv. Mater.* **2015**, *27*, 7162-7167.
(7) Eaton, S. W.; Lai, M. L.; Gibson, N. A.; Wong, A. B.; Dou, L. T.; Ma, J.; Wang, L. W.; Leone, S. R.; Yang, P. D. Lasing in Robust Cesium Lead Halide Perovskite Nanowires. *P. Natl. Acad. Sci.* **2016**, *113*, 1993-1998.
(8) Ramasamy,P.; Lim, D. H.; Kim, B.; Lee, S. H.; Lee, M. S.; Lee, J. S. All-inorganic Cesium Lead Halide Perovskite Nanocrystals for Photodetector Applications. *Chem. Commun.* **2016**, *52*, 2067-2070.
(9) Song, X. F.; Liu, X. H.; Yu, D. J.; Huo, C. X.; Ji, J. P.; Li, X. M.; Zhang, S. L.; Zou, Y. S.; Zhu, G. Y.; Wang, Y. J.; Wu, M. Z.; Xie, A.; Zeng, H. B et.al. Boosting Two-Dimensional $MoS_2/CsPbBr_3$ Photodetectors via Enhanced Light Absorbance and Interfacial Carrier Separation. *ACS. Appl. Mater. Inter.* **2018**, *10*, 2801-2809.
(10) Pan, A. Z.; Wang, J. L.; Jurow, M. J.; Jia, M. J.; Liu, Y.; Wu, Y. S.; Zhang, Y. F.; He, L.; Liu, Y. General Strategy for the Preparation of Stable Luminous Nanocomposite Inks Using Chemically Addressable $CsPbX_3$ Peroskite Nanocrystals. *Chem. Mater.* **2018**, *30*, 2771-2780.
(11) Shoaib, M.; Zhang, X. H.; Wang, X. X.; Zhou, H.; Xu, T.; Wang, X.; Hu, X. L.; Liu, H. W.; Fan, X. P.; Zheng, W. H.; Yang, T. F.; Yang, S. Z.; Zhang, Q. L.; Zhu, X. L.; Sun, L. T.; Pan, A. L et.al. Directional Growth of Ultralong $CsPbBr_3$ Perovskite Nanowires for High-Performance Photodetectors. *J. Am. Chem. Soc.* **2017**, *139*, 15592-15595.
(12) Tang, X. S.; Zu, Z. Q.; Zang, Z. G.; Hu, Z. P.; Hu, W.; Yao, Z. Q.; Chen,W. W.; Li, S. Q.; Han, S.; Zhou, M. $CsPbBr_3$/Reduced Graphene Oxide Nanocomposites and Their Enhanced Photoelectric Detection Application. *Sensor Actuat. B-Chem.* **2017**, *245*, 435-440.
(13) Zou, T. Y.; Liu, X. Y.; Qiu, R. Z.; Wang, Y.; Huang, S. Y.; Liu, C.; Dai, Q.; Zhou, H. Enhanced UV-C Detection of Perovskite Photodetector Arrays via Inorganic $CsPbBr_3$ Quantum Dot Down-Conversion Layer. *Adv. Opt. Mater.*

2019, *7*, 1801812-180181819.
(14) Stoumpos, C. C.; Malliakas, C. D.; Peters, J. A.; Liu, Z. F.; Sebastian, M.; Im, J.; Chasapis, T. C.; Wibowo, A. C.; Chung, D. Y.; Freeman, A. J.; Wessels, B. W.; Kanatzidis, M. G et.al. Crystal Growth of the Perovskite Semiconductor $CsPbBr_3$: A New Material for High-Energy Radiation Detection. *Cryst. Growth Des.* **2013**, *13*, 2722-2727.
(15) He, Y. H.; Matei, L.; Jung, H. J.; McCall, K. M.; Chen, M.; Stoumpos, C. C.; Liu, Z. F.; Peters, J. A.; Chung, D. Y.; Wessels, B. W.; Wasielewski, M. R.; Dravid, V. P.; Burger, A.; Kanatzidis, M. G et.al. High Spectral Resolution of Gamma-rays at Room Temperature by Perovskite $CsPbBr_3$ Single Crystals. *Nat. Commun.* **2018**, *9*, 1609-1616.
(16) Zhang, H.; Zhan, Z. H.; Ma, C.; Liu, Y. Q.; Xie, H. P.; Luo, S. Q.; Yuan, Y. B.; Gao, Y. L.; Zhang, Y.; Ming, W. Q.; Liu, Y.; Pan, A. L.; Yang, B et.al. Low-temperature Synthesis of All-inorganic Perovskite Nanocrystals for UV-photodetectors. *J. Mater. Chem. C* **2019**, *7*, 5488-5496.
(17) Liu, H.; Neal, A. T.; Zhu, Z.; Luo, Z.; Xu, X. F.; Tomanek, D.; Ye, P. D. Phosphorene: An Unexplored 2D Semiconductor with a High Hole Mobility. *ACS Nano* **2014**, *8*, 4033-4041.
(18) Novoselov, K. S.; Fal'ko, V. I.; Colombo, L.; Gellert, P. R.; Schwab, M. G.; Kim, K. A Roadmap for Graphene. *Nature* **2012**, *490*, 192-200.
(19) Naguib, M.; Kurtoglu, M.; Presser, V.; Lu, J.; Niu, J. J.; Heon, M.; Hultman, L.; Gogotsi, Y.; Barsoum, M. W. Two-Dimensional Nanocrystals Produced by Exfoliation of Ti_3AlC_2. *Adv. Mater.* **2011**, *23*, 4248-4253.
(20) Chen, C.; Xie, X. Q.; Anasori, B.; Sarycheva, A.; Makaryan, T.; Zhao, M. Q.; Urbankowski, P.; Miao, L.; Jiang, J. J.; Gogotsi, Y. MoS_2-on-MXene Heterostructures as Highly Reversible Anode Materials for Lithium-Ion Batteries. *Angew. Chem. Int. Edit.* **2018**, *57*, 1846-1850.
(21) Xu, Y. F.; Yang, M. Z.; Chen, B. X.; Wang, X. D.; Chen, H. Y.; Kuang, D. B.; Su, C. Y. A $CsPbBr_3$ Perovskite Quantum Dot/Graphene Oxide Composite for Photocatalytic CO_2 Reduction. *J. Am. Chem. Soc.* **2017**, *139*, 5660-5663.
(22) Muduli, S.; Pandey, P.; Devatha, G.; Babar, R.; Thripuranthaka, M.;

Kothari, D. C.; Kabir, M.; Pillai, P. P.; Ogale, S. Photoluminescence Quenching in Self-Assembled $CsPbBr_3$ Quantum Dots on Few-Layer Black Phosphorus Sheets. *Angew. Chem. Int. Edit.* **2018**, *57*, 7682-7686.

(23) Ou, M.; Tu, W. G.; Yin, S. M.; Xing, W. N.; Wu, S. Y.; Wang, H. J.; Wan, S. P.; Zhong, Q.; Xu, R. Amino-Assisted Anchoring of $CsPbBr_3$ Perovskite Quantum Dots on Porous g-C_3N_4 for Enhanced Photocatalytic CO_2 Reduction. *Angew. Chem. Int. Edit.* **2018**, *57*, 13570-13574.

(24) Huang, H.; Li, J.; Yi, Y.; Wang, J. H.; Kang, Y. H.; Chu, P. K.; Ong, H. C.; Yu, X. F. In Situ Growth of All-inorganic Perovskite Nanocrystals on Black Phosphorus Nanosheets. *Chem. Commun.* **2018**, *54*, 2365-2368.

(25) Anasori, B.; Lukatskaya, M. R.; Gogotsi, Y. 2D Metal Carbides and Nitrides (MXenes) for Energy Storage. *Nat. Rev. Mater.* **2017**, *2, 16098-16114.*

(26) Seh, Z. W.; Fredrickson, K. D.; Anasori, B.; Kibsgaard, J.; Strickler, A. L.; Lukatskaya, M. R.; Gogotsi, Y.; TJaramillo, F.; Vojvodic, A. Two-Dimensional Molybdenum Carbide (MXene) as an Efficient Electrocatalyst for Hydrogen Evolution. *ACS Energy Lett.* **2016**, *1*, 589-594.

(27) Meng, R. J.; Huang, J. M.; Feng, Y. T.; Zu, L. H.; Peng, C. X.; Zheng, L. R.; Zheng, L.; Chen, Z. B.; Liu, G. L.; Chen, B. J.; Mi, Y. L.; Yang, J. H et.al. Black Phosphorus Quantum Dot/Ti_3C_2 MXene Nanosheet Composites for Efficient Electrochemical Lithium/Sodium-Ion Storage. *Adv. Energy Mater.* **2018**, *8,* 589-594.

(28) Xue, Q.; Zhang, H. J.; Zhu, M. S.; Pei, Z. X.; Li, H. F.; Wang, Z. F.; Huang, Y.; Huang, Y.; Deng, Q. H.; Zhou, J.; Du, S. Y.; Huang, Q.; Zhi, C. Y et.al. Photoluminescent Ti_3C_2 MXene Quantum Dots for Multicolor Cellular Imaging. *Adv. Mater.* **2017**, *29*, 1604847-1604853.

(29) Ding, L.; Wei, Y. Y.; Li, L. B.; Zhang, T.; Wang, H. H.; Xue, J.; Ding, L. X.; Wang, S. Q.; Caro, J.; Gogotsi, Y. MXene Molecular Sieving Membranes for Highly Efficient Gas Separation. *Nat. Commun.* **2018**, *9,* 155-161.

(30) Alhabeb, M.; Maleski, K.; Mathis, T. S.; Sarycheva, A.; Hatter, C. B.; Uzun, S.; Levitt, A.; Gogotsi, Y. Selective Etching of Silicon from Ti_3SiC_2 (MAX) To Obtain 2D Titanium Carbide (MXene). *Angew. Chem. Int. Edit.* **2018**, *57*,

5444-5448.
(31) Cao, S. W.; Shen, B. J.; Tong, T.; Fu, J. W.; Yu, J. G. 2D/2D Heterojunction of Ultrathin MXene/Bi_2WO_6 Nanosheets for Improved Photocatalytic CO_2 Reduction. *Adv. Funct. Mater.* **2018**, *28,* 1800136-1800146.
(32) Fan, Z. M.; Wang, Y. S.; Xie, Z. M.; Wang, D. L.; Yuan, Y.; Kang, H. J.; Su, B. L.; Cheng, Z. J.; Liu, Y. Y. Modified MXene/Holey Graphene Films for Advanced Supercapacitor Electrodes with Superior Energy Storage. *Adv. Sci.* **2018**, *5,* 1800750-1800760.
(33) Burstein, E. Anomalous Optical Absorption Limit in Insb. *Phys. Rev.* **1954**, *93*, 632-633.
(34) Moss, T. S. The Interpretation of the Properties of Indium Antimonide. *P. Phys. Soc. Lond. B* **1954**, *67*, 775-782.
(35) Begum, R.; Parida, M. R.; Abdelhady, A. L.; Murali, B.; Alyami, N. M.; Ahmed, G. H.; Hedhili, M. N.; Bakr, O. M.; Mohammed, O. F. Engineering Interfacial Charge Transfer in $CsPbBr_3$ Perovskite Nanocrystals by Heterovalent Doping. *J. Am. Chem. Soc.* **2017**, *139*, 731-737.
(36) Deng, W.; Huang, H. C.; Jin, H. M.; Li, W.; Chu, X.; Xiong, D.; Yan, W.; Chun, F. J.; Xie, M. L.; Luo, C.~~; Jin, L.; Liu, C. Q.; Zhang, H. T.; Deng, W. L.; Yang, W. Q et.al~~. All-Sprayed-Processable, Large-Area, and Flexible Perovskite/MXene-Based Photodetector Arrays for Photocommunication. *Adv. Opt. Mater.* **2019**, *7*, 1801521-1801529.
(37) Wang, Z. W.; Kim, H.; Alshareef, H. N. Oxide Thin-Film Electronics using All-MXene Electrical Contacts. *Adv. Mater.* **2018**, *30,* 1706656-1706662.
(38) Song, J. Z.; Xu, L. M.; Li, J. H.; Xue, J.; Dong, Y. H.; Li, X. M.; Zeng, H. B. Monolayer and Few-Layer All-Inorganic Perovskites as a New Family of Two-Dimensional Semiconductors for Printable Optoelectronic Devices. *Adv. Mater.* **2016**, *28*, 4861-4869.
(39) Hou, J. G.; Cao, S. Y.; Wu, Y. Z.; Gao, Z. M.; Liang, F.; Sun, Y. Q.; Lin, Z. S.; Sun, L. C. Inorganic Colloidal Perovskite Quantum Dots for Robust Solar CO_2 Reduction. *Chem-Eur. J.* **2017**, *23*, 9481-9485.

(40) Kong, Z. C.; Liao, J. F.; Dong, Y. J.; Xu, Y. F.; Chen, H. Y.; Kuang, D. B.; Su, C. Y. Core@Shell $CsPbBr_3$@Zeolitic Imidazolate Framework Nanocomposite for Efficient Photocatalytic CO_2 Reduction. *ACS Energy Lett.* **2018**, *3*, 2656-2662.
(41) Xu, Y. F.; Wang, X. D.; Liao, J. F.; Chen, B. X.; Chen, H. Y.; Kuang, D. B. Amorphous-TiO_2-Encapsulated $CsPbBr_3$ Nanocrystal Composite Photocatalyst with Enhanced Charge Separation and CO_2 Fixation. *Adv. Mater. Interfaces.* **2018**, *5,* 1801015-1801022.
(42) Wan, S. P.; Ou, M.; Zhong, Q.; Wang, X. M. Perovskite-type $CsPbBr_3$ Quantum Dots/UiO-66(NH_2) Nanojunction as Efficient Visible-light-driven Photocatalyst for CO_2 Reduction. *Chem. Eng. J.* **2019**, *358*, 1287-1295.